ACS APPLIED MATERIALS & INTERFACES

Research Article

www.acsami.org

# Palladium-Decorated Hydrogen-Gas Sensors Using Periodically Aligned Graphene Nanoribbons

Yusin Pak,[†] Sang-Mook Kim,[‡] Huisu Jeong,[†] Chang Goo Kang,[†] Jung Su Park,[§] Hui Song,[†] Ryeri Lee,[†] NoSoung Myoung,[§] Byoung Hun Lee,[†] Sunae Seo,[∥] Jin Tae Kim,*[,⊥] and Gun-Young Jung*[,†]

[†]School of Materials Science and Engineering and [§]Advanced Photonics Research Institute, Gwangju Institute of Science and Technology, 261 Cheomdan-gwagiro, Buk-gu, Gwangju 500-712, Republic of Korea

[‡]Korea Photonics Technology Institute, Chumdan 4-ro 5, Buk-gu, Gwangju 500-779, Republic of Korea

[∥]Department of Physics and Graphene Research Institute, Sejong University, 98 Gunja-dong, Gwangjin-gu, Seoul 143-747, Republic of Korea

[⊥]Creative Future Research Laboratory, Electronics and Telecommunications Research Institute, 218 Gajeong-ro, Yuseong, Daejeon 305-700, Republic of Korea

Supporting Information

**ABSTRACT:** Polymer residue-free graphene nanoribbons (GNRs) of 200 nm width at 1 $\mu$m pitch were periodically generated in an area of 1 cm$^2$ via laser interference lithography using a chromium interlayer prior to photoresist coating. High-quality GNRs were evidenced by atomic force microscopy, micro-Raman spectroscopy, and X-ray photoelectron spectroscopy measurements. Palladium nanoparticles were then deposited on the GNRs as catalysts for sensing hydrogen gases, and the GNR array was utilized as an electrically conductive path with less electrical noise. The palladium-decorated GNR array exhibited a rectangular sensing curve with unprecedented rapid response and recovery properties: 90% response within 60 s at 1000 ppm and 80% recovery within 90 s in nitrogen ambient. In addition, reliable and repeatable sensing behaviors were revealed when the array was exposed to various gas concentrations even at 30 ppm.

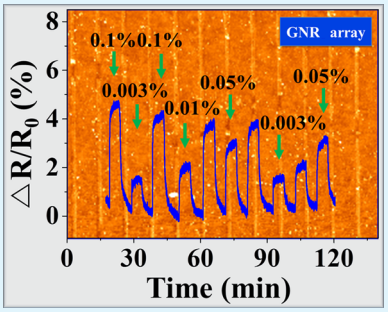


**KEYWORDS:** *graphene nanoribbons, interference lithography, hydrogen-gas sensor, fast response and recovery*

## 1. INTRODUCTION

Hydrogen has potential as an ecofriendly resource for many applications in future science and industry; however, there is a serious safety concern. Excellent monitoring and leak detector systems are required because hydrogen is invisible, odorless, and highly flammable.

Conventional hydrogen-gas sensors based on metal oxides ($In_2O_3$, $SnO_2$, ZnO, NiO, and $TiO_2$)[1−4] have decent sensitivities, but their high-temperature performance at approximately 400 °C is a significant drawback. Accordingly, palladium (Pd) is considered to be an attractive material because of its superior hydrogen solubility at room temperature. However, hydrogen sensors based on a Pd film are vulnerable to structural transformations (vacancies and dislocations), which are accelerated during the phase transition of $Pd_\alpha$ to $Pd_\beta$ that occurs at hydrogen concentrations greater than 2%, causing a Pd film buckling.[5−8] In addition, the low hydrogen diffusion coefficient ($3.8 \times 10^{-7}$ cm$^2$/s at 298 K) of the Pd film[9] can result in a long response time especially at low hydrogen concentrations below 1%.[10]

To overcome these problems, researchers have focused their attention on various Pd nanostructures such as nanowires,[11−13] nanochains,[14] nanotubes,[15] and nanocomposites.[16] Among these, one-dimensional Pd nanowire hydrogen sensors[11−13] give better performances in terms of sensitivity and power consumption. Meanwhile, the recent discovery of graphene[17] opened up the possibility of utilizing zero-dimensional Pd nanoparticles (Pd-NPs), which have the highest surface area among all other dimensional structures mentioned above. Therefore, sensors utilizing a pristine chemical vapor depostion (CVD)-grown graphene[18,19] or graphene oxide[16] layers as a conductive platform covered with uniformly dispersed Pd-NPs have also been investigated.

Recently, enhanced hydrogen-sensing properties were achieved with a Pd-decorated graphene nanoribbon (GNR)-networked porous film (55% sensitivity at 40 ppm along with a 50% response time of 21 s and a 50% recovery time of 23 s in air)[20] and a Pd-decorated carbon-nanotube-woven porous film (0.4% sensitivity at 100 ppm along with a 90% response time of 18 min and a 90% recovery time of 20 min in air).[21] Such films are advantageous for large area detection, but the solution filtering process to produce such porous films makes it difficult to control the density and arrangement of one-dimensional composites, which directly corresponds to the number of hydrogen adsorptive sites within the film. This is inadequate for reliable and repeatable sensing behavior. Furthermore, such

Received: May 21, 2014
Accepted: July 22, 2014
Published: July 22, 2014

  

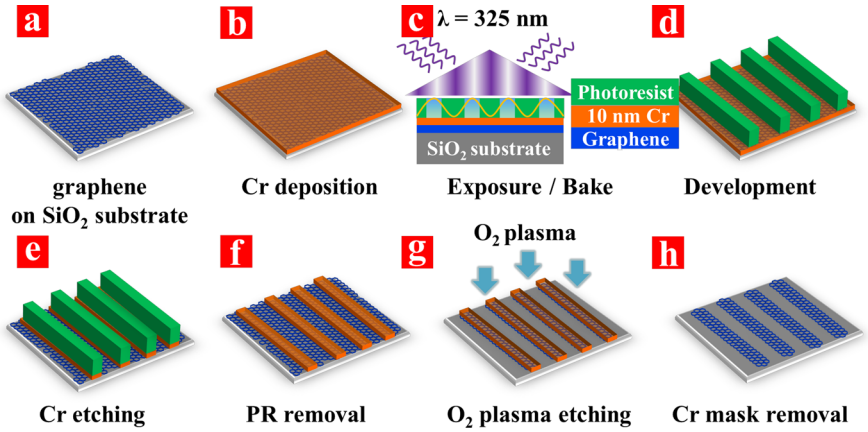


**Figure 1.** Fabrication processes of the GNR array. (a) Preparation of the monolayer graphene/$SiO_2$ substrate. (b) Deposition of a 10-nm-thick Cr layer by electron-beam evaporation. (c) Spin coating of an AZ GXR 601 PR on the Cr/graphene/$SiO_2$ substrate followed by exposure to a 325 nm interfered laser. (d) Development to produce the PR line pattern. (e) Wet etching of the underlying Cr layer. (f) Removal of the PR with acetone. (g) Oxygen plasma treatment to etch the underlying graphene layer with the Cr line etching mask. (h) Removal of the Cr line etching mask to reveal the GNR array.

dense and nonaligned composites within the film cause a slow and incomplete recovery unless hydrogen-desorption-enhancing air is supplied.[22]

Therefore, hydrogen sensors with rapid response at low concentrations and fast recovery without using hydrogen-desorption-enhancing agents must be developed. To accomplish this, the graphene area must be controlled by lithographic techniques, which has not been demonstrated in graphene-based hydrogen sensors because of unavoidably remaining photoresist (PR) residue on the graphene surface, deteriorating gas sensor performances. Comparative table and graphs for sensitivities and response times of various Pd-based hydrogen sensors can be found in the Supporting Information (SI), section S1.

In this work, a periodically aligned GNR (200 nm width) array with no polymer residue was faithfully produced by placing a chromium (Cr) interlayer under the PR via 325 nm laser interference lithography[23] and then incorporating it into the Pd-decorated hydrogen sensors. This sensor demonstrated a rapid response (90% within 60 s) at 1000 ppm and recovery (80% within 90 s) in nitrogen ambient along with reliable repeatability at various concentrations even at 30 ppm.

## 2. EXPERIMENTAL SECTION

**Preparation of Single-Layer Graphene on a $SiO_2$ Substrate.** Graphene was grown on a 300-nm-thick copper/nickel (Cu/Ni) film on a $SiO_2$/silicon (Si) wafer by inductively coupled plasma chemical vapor deposition (ICP-CVD). The substrate temperature was ramped up from room temperature to 650 °C at a base pressure of $5 \times 10^{-7}$ Torr. The wafer surface was cleaned with a radio-frequency plasma source under flowing hydrogen gas. The graphene was grown for 3 min in a gas mixture of argon and acetylene with a plasma power of 100 W.[24]

After cooling, the CVD-grown graphene was transferred to another $SiO_2$/n-type Si wafer. First, poly(methyl methacrylate) (PMMA) was spin-coated onto the grown graphene layer and baked for 1 min at 180 °C. After baking, the metal layers were etched away by soaking the wafer in a $FeCl_3$ solution for 3 h for a floating PMMA/graphene film. The floating PMMA/graphene film was lifted onto poly(ethylene terephthalate) film, soaked in a deionized water bath for 15 min, and then transferred to the $SiO_2$ substrate. The samples were dried on a hot plate at 60 °C for 2 h and finally cleaned in an acetone bath to remove PMMA.

**325 nm Laser Interference Lithography and Pattern Transfer to Graphene.** An AZ GXR 601 positive tone PR (AZ Electronics Materials) was diluted with an AZ 1500 thinner (1:0.8 volume ratio) and then spin-coated at 4500 rpm onto the 10-nm-thick Cr film/graphene substrate. The 10-nm-thick Cr layer was deposited by an electron-beam evaporator at a rate of 0.1 Å/s under a pressure of $10^{-6}$ Torr. After prebaking at 115 °C for 1 min, the AZ GXR 601 PR/Cr film/graphene substrate was exposed to a 325 nm laser interference system with a dose of 32 mJ/cm$^2$. Half of a diffracted laser light through a 10 $\mu$m pinhole irradiated the PR directly, and the other half projected the PR after being reflected at a Lloyd's mirror, which was placed perpendicular to the sample. These two beams interfered at a certain angle of 9.35° to generate a PR line pattern at 1 $\mu$m pitch according to $\Lambda = \lambda/2 \sin\theta$, where $\lambda$ is the wavelength and $\theta$ is the half-angle between the two beams.

After exposure, the sample was developed in an MIF 300 solution (AZ Electronics Materials) for 40 s and then baked at 100 °C for 30 s. To remove the PR residue after development, oxygen plasma etching was performed with 50 sccm of $O_2$, 20 mTorr, and 20 W for 30 s. The generated PR line pattern was transferred to the underlying Cr layer by dipping in a Cr etchant (CR-7, Cyantek Corp.) for 40 s and rinsed in a water bath for 2 min. The single graphene layer was subsequently plasma-etched with 50 sccm of $O_2$ and 100 W for 40 s. Finally, the Cr mask was stripped away with the CR-7 etchant to expose the underlying periodic GNRs.

## 3. RESULTS AND DISCUSSION

Figure 1 depicts the scheme for fabricating the GNR array via 325 nm helium−cadmium laser interference lithography, which is generally considered to be a very simple, rapid, inexpensive, and maskless method for producing periodic nanoscale patterns over a large area. The direct coating of the PR to the graphene layer usually leaves a polymer residue on the graphene surface, which cannot be removed without thermal annealing, causing strains or doping in the graphene layer.[25]

Therefore, to avoid direct contact of the PR to the graphene layer, a metal layer was inserted between them. Various metals [gold (Au), platinum (Pt), aluminum (Al), Ni, and Cr)] were deposited via electron-beam evaporation. A 10-nm-thick Cr film was chosen as the best, on which nanoscale PR lines were faithfully created after development and transferred to the Cr layer with the Cr etchant. The Pt and Al films came off the substrate during development because of poor adhesion to the graphene surface. The Au and Ni films were dissolved too

quickly in their etchants (aqua regia and $FeCl_2$ solution, respectively) without reliable pattern transfer.

Figure 2a shows a scanning electron microscopy (SEM) image of the periodically aligned PR line pattern with a 200 nm width at a pitch of 1 $\mu$m after development. Figure 2b shows the Cr line pattern produced faithfully after pattern transfer with the CR-7 solution for 40 s (see the SI, section S2). Atomic force microscopy (AFM) measurements were performed to qualify the GNR array. Parts c and d of Figure 2 show the AFM images of GNR arrays fabricated with and without the Cr interlayer, respectively. The GNR array generated using the Cr interlayer was as clean as the pristine graphene surface (inset in Figure 2c) without any conspicuous polymer residue. In contrast, the GNR array produced by the direct coating of the PR was covered with much residue with a height of 4 nm on average along the lines (Figure 2d). This residue could be reduced by a long period of polymer stripping and subsequent annealing, which could peel off or damage the thin graphene layer undesirably. This study indicates that the Cr interlayer can be utilized effectively for obtaining PR residue-free graphene patterns.

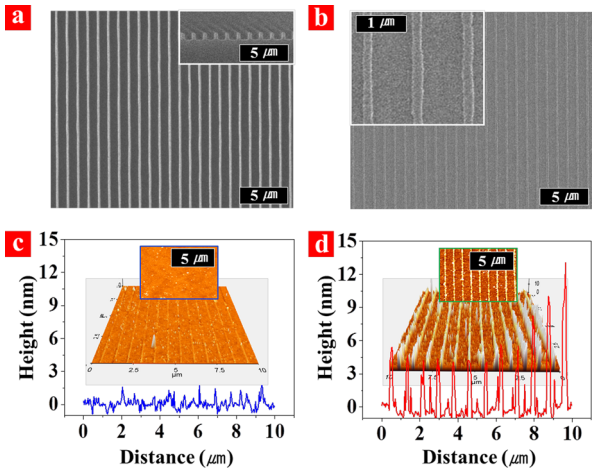


**Figure 2.** (a) SEM image of the periodically aligned PR lines with a 200 nm line width at a pitch of 1 $\mu$m. The inset shows the cross-sectional view of PR lines with 500 nm height. (b) SEM image of the periodically aligned Cr lines with 200 nm width. (c) AFM image of the GNR array fabricated by using the Cr interlayer with a surface profile of less than 1 nm. Inset: AFM image of the pristine graphene for comparison. (d) AFM image of the GNR array fabricated without the Cr interlayer. The surface profile shows the presence of a thick PR residue. Inset: top view of this AFM image.

Both micro-Raman spectroscopy and X-ray photoelectron spectroscopy were also measured with the two samples. Figure 3a shows a Raman spectrum of the CVD-grown graphene with a small D peak at 1345 $cm^{-1}$, a sharp G peak at 1597 $cm^{-1}$, and an intense 2D peak at 2688 $cm^{-1}$. Both the relative peak ratios among the G, D, and 2D bands and the 2D band shape can determine the graphene quality.[26,27] The measured D/G and G/2D ratios of the pristine graphene are 0.1 and 0.4, respectively, and the 2D peak (inset figure) is closely fitted by a single-component symmetric Lorentzian function, suggesting that the CVD-grown graphene was single layer with few structural defects.[28]

The micro-Raman spectrum of the GNR array (Figure 3b) also contains the same D, G, and 2D peaks. The 2D peak of the GNRs (inset figure) is still fitted by the Lorentzian function,

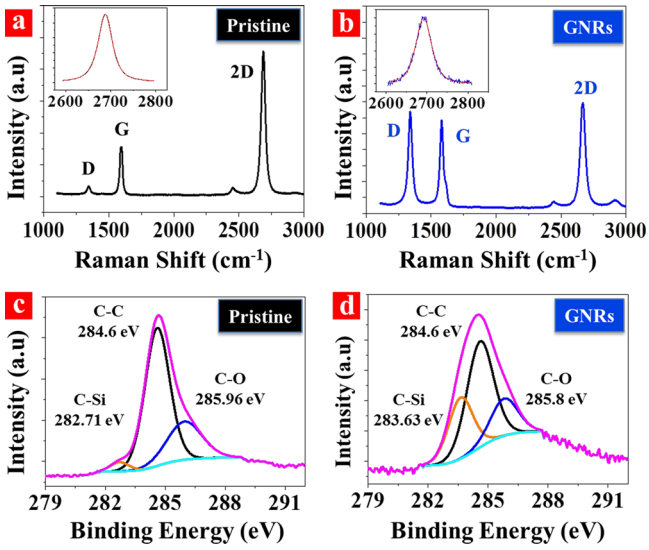


**Figure 3.** Micro-Raman spectra of (a) the pristine graphene and (b) the GNR array. X-ray photoelectron spectra of (c) the pristine graphene and (d) the GNR array.

but both the D/G and G/2D ratios are close to 1. This ratio increase indicates that structural changes occurred in the GNRs mainly because of the increased open edges. This has also been reported in other lithographically patterned GNRs;[29,30] in those cases, a significant peak caused by the PR residue occurred between the D and G bands,[29] which was not evident in our study. Likewise, the Raman spectrum of the GNR array fabricated by the direct coating of the PR on the graphene surface revealed a significant polymer residue peak, overlapped with the D band (SI, section S3).

The X-ray photoelectron spectroscopy results shown in Figure 3c,d support the above Raman spectroscopy results. The C 1s peak of the C−C bonds is clearly seen at approximately 284.6 eV[31] for both samples. The peak of the C−O bonds at 285.96 eV can be affected by the unintentional adsorption of hydrocarbons from ambient air.[32] The peak ratio of the C−C bonds to the C−O bonds is 1:0.28 for the pristine graphene but becomes 1:0.58 for the GNR array because of the patterning-induced graphene area reduction. Neither newly created nor significantly altered bonds were observed, confirming that our lithographic process holds great potential for high-quality graphene patterns.

To fabricate hydrogen sensors, 2-nm-thick Pd was deposited across the entire sample (SI, section S4) and 90-nm-thick Au electrodes were deposited by an electron-beam evaporator using a shadow mask. The electrode gap and length were 50 and 5000 $\mu$m, respectively. A total of 1000 GNRs were connected between the two electrodes considering the 1 $\mu$m pitch. For a direct comparison, the pristine graphene film was also deposited with a 2-nm-thick Pd and subjected to the same sensor fabrication.

We constructed a homemade measurement setup for hydrogen-gas sensing (SI, section S5) with a sample location in the middle of a quartz tube to maintain a constant gas stream for a stable gas reaction. Every analysis was performed under the same conditions (room temperature, 30% humidity, at 0.01 V). At first, highly pure nitrogen gas (99.999%) was supplied to the tube at 1800 sccm for 15 min to have a stable current level and rule out any other reactive gas molecules.[22] After a certain stable current level was reached, hydrogen gas was supplied

with various concentrations (1000, 500, 100, and 30 ppm). Sensitivity is defined as

$$S\ (\%) = (R_s - R_i)/R_i \times 100$$

where $R_s$ is the saturated resistance in the presence of hydrogen gas and $R_i$ is the initial resistance. To measure the recovery, the hydrogen flow was stopped and only nitrogen gas was flowing. The recovery of hydrogen-gas sensors in nitrogen ambient is slow or incomplete. Therefore, in many previous studies, a recovery-enhancing gas such as oxygen was necessarily supplied to expedite recovery via a condensation reaction ($2H_2 + O_2 \rightarrow H_2O$).[33] In this study, however, no recovery-enhancing gas was utilized to evaluate the natural desorption of hydrogen molecules from Pd-decorated GNR sensors.

Parts a and b of Figure 4 show the sensitivity as a function of time for the pristine and 200-nm-wide GNR sensors,

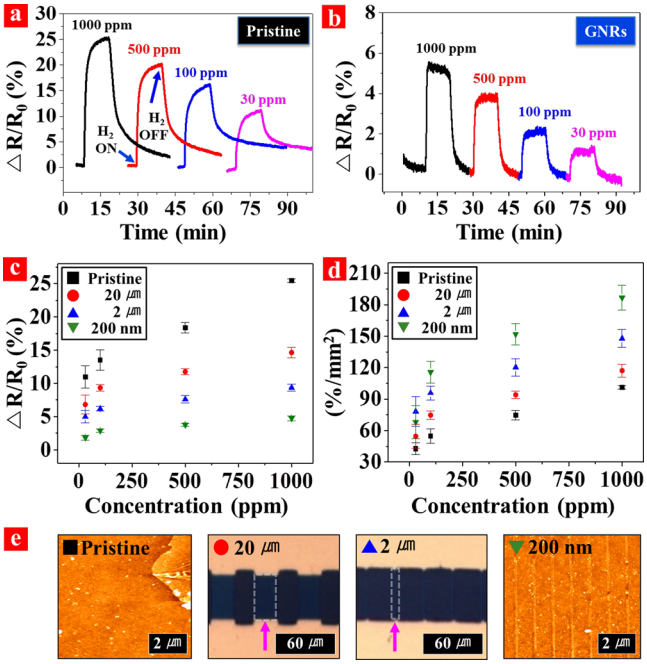


**Figure 4.** Pd-decorated hydrogen-gas-sensor performance: sensitivity change of (a) the pristine graphene sensor and (b) the GNR array sensor at different concentrations. (c) Comparison of the sensitivities among the four samples with different graphene widths (pristine, 20 $\mu$m, 2 $\mu$m and 200 nm). (d) Comparison of the areal sensitivities at different concentrations. (e) Optical (20 and 2 $\mu$m) and AFM (pristine and 200 nm) images of graphene patterns in the four samples. The arrow indicates the location of graphene ribbon.

respectively, at hydrogen-gas concentrations ranging from 30 to 1000 ppm. When hydrogen gas was injected (on state), the sensitivity of the pristine sensor increased, reached a saturation of approximately 25% at 1000 ppm, but seemed to still rise slowly afterward. When the hydrogen flow was stopped (off state), it started to decrease and approached its initial resistance after a substantial time, which became much longer in the case of lower concentrations. The increase of hydrogen-initiated resistance is due to palladium hydride formation.[34] When hydrogen molecules meet the Pd-NPs deposited on the graphene, the work function of Pd decreases. Therefore, electrons are transferred to the graphene, depleting the major hole carriers in the graphene and thus increasing the resistance.

The adsorption ($r_a$) and desorption ($r_d$) rates of gas molecules[35] in gas sensors are defined as

$$r_a = k_a C(1 - \Omega)^2, \qquad r_d = k_d \Omega^2$$

where $k_a$ and $k_d$ are the adsorption and desorption rate constants, respectively. Because the surface fraction occupied by hydrogen molecules ($\Omega$) is negligible initially, the initial response rate is linearly related to the concentration ($C$) but slows down by $(1 - \Omega)^2$ with hydrogen adsorption. The recovery rate is directly related to $\Omega^2$. After the sensitivity reaches saturation, the initial recovery rate is high because of the large value of $\Omega$ but slows down substantially with hydrogen desorption, creating the common shark-fin gas-sensing behavior as shown in the pristine sensors. The shark-fin sensing behavior becomes more prominent at a lower concentration, as shown in Figure 4a. This behavior has been demonstrated in previous gas-sensor studies.[18,21] In comparison, the GNR sensors had a square response and recovery curve rather than the shark-fin curve. Interestingly, it exhibited a fast and complete recovery even at 30 ppm in nitrogen ambient without using the air that had been used to facilitate swift recovery. The GNR sensor had a lower sensitivity mainly because of the reduced number of Pd-NPs deposited on the narrow GNRs. On the other hand, the GNR sensor was advantageous for speedy response and recovery because fewer gas molecules were adsorbed and desorbed easily at the reduced number of Pd-NPs, leading to the square-type sensing behavior.

Two additional samples having micron-scale graphene ribbon arrays (20 and 2 $\mu$m width) were fabricated with the same electrode configuration by photolithography using the Cr interlayer, and their sensing properties were measured. Figure 4c compares the sensitivities among the four samples (pristine, 20 $\mu$m, 2 $\mu$m and 200 nm) at different concentrations. The sensitivity at each concentration decreased with the reduction of the ribbon width, which corresponds to the reduction in the number of Pd-NPs. Areal sensitivities, newly defined as the sensitivity divided by the total graphene area between electrodes, are compared in Figure 4d. There was little difference in the areal sensitivity among the samples at 30 ppm, but it became distinctive with increasing concentration. This indicates that most hydrogen molecules at low concentration are easily adsorbed onto the active sites of Pd-NPs regardless of the graphene area. At higher concentrations, the limited active sites of the 200 nm sensor are quickly occupied by the affluent hydrogen molecules. In contrast, in the case of the pristine sensor, the graphene area is comparatively large enough that all of the active sites of Pd-NPs residing on it are not consumed promptly right after gas exposure.

Figure 5a compares the sensitivity change for 50 min exposure to 1000 ppm, showing the usual shark-fin behavior in the pristine sensor and the square behavior in the 200 nm GNR sensor, respectively. The sensitivity of the GNR sensor reached 90% of its saturated value within 60 s and remained constant during the measurement along with a rapid recovery to the base current even in nitrogen ambient. This unprecedented fast response and recovery behavior is attributed to the limited number of Pd-NPs, which facilitate facile gas molecule adsorption and desorption. In comparison, the sensitivity of the pristine sensor increased quickly at first but then saturated slowly. It took 8 min 30 s to reach 80% of its saturated value and became saturated after 50 min. The pristine sensor was recovered by 80% (25% → 5%) in 18 min 40 s after the gas was

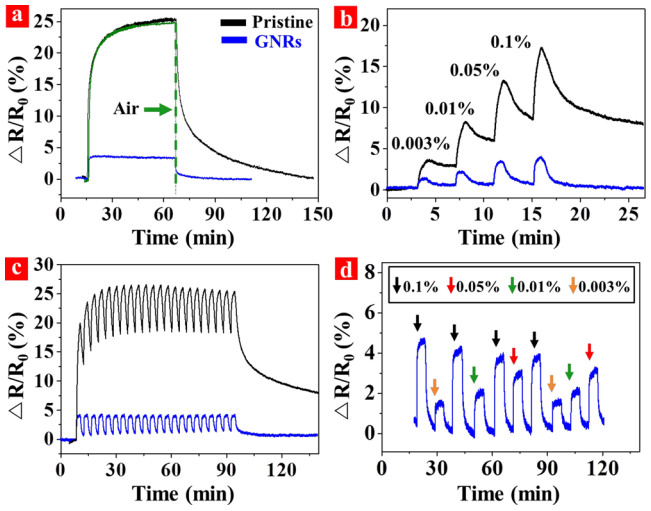


**Figure 5.** In-depth analysis of the hydrogen-gas-sensor performance at various on/off cycles. (a) Long hydrogen-gas exposure (on, 50 min) experiment. (b) 4 cycles of 30 s response (on) and 2 min recovery (off) with incrementally increasing concentrations. (c) Repeatability test. There were 22 cycles of 2 min response and 2 min recovery. (d) Reliability test. The GNR sensor was exposed to arbitrary concentrations with cycles of 5 min response and 5 min recovery.

turned off, and an additional 70 min was required to return to the base current in nitrogen ambient. The recovery time decreased dramatically when air flow was utilized to pull the adsorbed hydrogen molecules out by condensation, as indicated with a green curve in Figure 5a. Meanwhile, the GNR sensor was recovered by 80% (4.5% → 1%) in 90 s.

A different time-resolved sensitivity measurement (Figure 5b) was carried out with 4 cycles of 30 s on-state for response, followed by 2 min off-state for recovery with incrementally increasing hydrogen concentration for each cycle. The pristine sensor did not return to the initial current within the short recovery time allotted prior to the next exposure to a higher concentration, leading to a stepwise-increasing sensitivity behavior. The GNR sensor, on the other hand, returned to the base current completely and was ready to detect a higher concentration in the next cycle.

To evaluate the repeatability, 22 cycles of 2 min on-state and 2 min off-state were performed at 1000 ppm (Figure 5c). The GNR sensor had a good repeatability, demonstrating a fast and stable on/off switching in each cycle. The pristine sensor, in contrast, approached its saturated value after 5 cycles and hardly recovered more than 30% within the permitted 2 min. Utilizing these advanced response and recovery properties, the GNR sensor was exposed to arbitrary concentrations with 5 min on-state and 5 min off-state. The GNR sensor showed a fairly consistent sensitivity for each concentration regardless of the prior concentration to which it had been exposed (Figure 5d).

## 4. CONCLUSIONS

In summary, we successfully fabricated a periodically aligned 200-nm-wide GNR array at 1 $\mu$m pitch with no PR residue by implementing a 10-nm-thick Cr interlayer to protect the graphene surface from PR contamination. Pd-decorated GNR hydrogen-gas sensors produced by this method demonstrated reliable and repeatable sensor behaviors as well as rapid response and recovery behaviors: 90% response within 60 s at 1000 ppm and 80% recovery within 90 s in nitrogen ambient. Our method demonstrates a practical approach for producing residue-free nanoscale graphene patterns and a potential for creating efficient graphene-based devices.

## ■ ASSOCIATED CONTENT

### Supporting Information

Comparative table and graphs for sensitivities and response times of various Pd-based sensors, pattern transfer from the PR line mask to the Cr film, Raman spectra of the GNR array with/without the PR residue, Pd deposition and its characterization, gas sensitivity measurement setup, and response and recovery time for 40%, 60%, and 80% performance of both the pristine and GNR sensors. This material is available free of charge via the Internet at http://pubs.acs.org.

## ■ AUTHOR INFORMATION

### Corresponding Authors

*E-mail: jintae@etri.re.kr.

*E-mail: gyjung@gist.ac.kr.

### Author Contributions

The manuscript was written through contributions of all authors. All authors have given approval to the final version of the manuscript.

### Notes

The authors declare no competing financial interest.

## ■ ACKNOWLEDGMENTS

This work was supported by the Basic Science Research program through the National Research Foundation of Korea funded by the Ministry of Science, ICT & Future Planning (NRF Grant R15-2008-006-03002-0, CLEA, NCRC), the Pioneer Research Center Program (NRF Grant 2014M3C1A3016468), and the Ministry of Education (NRF Grant 2013R1A1A2061494) and a grant funded through the MEST (Grant 2011-0029414).

## ■ REFERENCES

(1) Varghese, O. K.; Gong, D.; Paulose, M.; Ong, K. G.; Grimes, C. A. Hydrogen Sensing Using Titania Nanotubes. *Sens. Actuators, B* **2003**, *93*, 338−344.

(2) Rout, C. S.; Krishna, S. H.; Vivekchand, S. R. C.; Govindaraj, A.; Rao, C. N. R. Hydrogen and Ethanol Sensors Based on ZnO Nanorods, Nanowires and Nanotubes. *Chem. Phys. Lett.* **2006**, *418*, 586−590.

(3) Wang, B.; Zhu, L. F.; Yang, Y. H.; Xu, N. S.; Yang, G. W. Fabrication of a $SnO_2$ Nanowire Gas Sensor and Sensor Performance for Hydrogen. *J. Phys. Chem. C* **2008**, *112*, 6643−6647.

(4) Lu, C.; Chen, Z. High-Temperature Resistive Hydrogen Sensor Based on Thin Nanoporous Rutile $TiO_2$ Film on Anodic Aluminum Oxide. *Sens. Actuators, B* **2009**, *140*, 109−115.

(5) Hughes, R. C.; Schubert, W. K.; Buss, R. J. Solid-State Hydrogen Sensors Using Palladium−Nickel Alloys: Effect of Alloy Composition on Sensor Response. *J. Electrochem. Soc.* **1995**, *142*, 249−254.

(6) Goltsova, M. V.; Artemenko, Yu. A.; Zaitsev, V. I. Kinetics and Morphology of the Reverse $\beta \rightarrow \alpha$ Hydride Transformation in Thermodynamically Open Pd−H System. *J. Alloys Compd.* **1999**, *293*−*295*, 379−384.

(7) Pundt, A. Hydrogen in Nano-sized Metals. *Adv. Eng. Mater.* **2004**, *6*, 11−22.

(8) Lee, E.; Lee, J. M.; Lee, E.; Noh, J.-S.; Joe, J. H.; Jung, B.; Lee, W. Hydrogen Gas Sensing Performance of Pd−Ni alloy Thin Films. *Thin Solid Films* **2010**, *519*, 880−884.

(9) Flanagan, T. B.; Oates, W. A. The Palladium−Hydrogen System. *Annu. Rev. Mater. Sci.* **1991**, *21*, 269−304.
(10) Yang, F.; Taggart, D. K.; Penner, R. M. Joule Heating a Palladium Nanowire Sensor for Accelerated Response and Recovery to Hydrogen Gas. *Small* **2010**, *6*, 1422−1429.
(11) Yang, F.; Taggart, D. K.; Penner, R. M. Fast, Sensitive Hydrogen Gas Detection Using Single Palladium Nanowires That Resist Fracture. *Nano Lett.* **2009**, *9*, 2177−2182.
(12) Offermans, P.; Tong, H. D.; Van Rijn, C. J. M.; Merken, P.; Brongersma, S. H.; Crego-Calama, M. Ultralow-Power Hydrogen Sensing with Single Palladium Nanowires. *Appl. Phys. Lett.* **2009**, *94*, 223110.
(13) Jeon, K. J.; Lee, J. M.; Lee, E.; Lee, W. Individual Pd Nanowire Hydrogen Sensors Fabricated by Electron-Beam Lithography. *Nanotechnology* **2009**, *20*, 135502.
(14) Favier, F.; Walter, E. C.; Zach, M. P.; Benter, T.; Penner, R. M. Hydrogen Sensors and Switches from Electrodeposited Palladium Mesowire Arrays. *Science* **2001**, *293*, 2227−2231.
(15) Yu, S.; Welp, U.; Hua, L. Z.; Rydh, A.; Kwok, W. K.; Wang, H. H. Fabrication of Palladium Nanotubes and Their Application in Hydrogen Sensing. *Chem. Mater.* **2005**, *17*, 3345−3450.
(16) Lange, U.; Hirsch, T.; Mirsky, V. M.; Wolfbeis, O. S. Hydrogen Sensor Based on a Graphene-Palladium Nanocomposite. *Electrochim. Acta* **2011**, *56*, 3707−3712.
(17) Geim, A. K.; Novoselov, K. S. The Rise of Graphene. *Nat. Mater.* **2007**, *6*, 183−191.
(18) Wu, W.; Liu, Z.; Jauregui, L. A.; Yu, Q.; Pillai, R.; Cao, H.; Bao, J.; Chen, Y. P.; Pei, S.-S. Wafer-Scale Synthesis of Graphene by Chemical Vapor Deposition and Its Application in Hydrogen Sensing. *Sens. Actuators, B* **2010**, *150*, 296−300.
(19) Chung, M. G.; Kim, D.-H.; Seo, D. K.; Kim, T.; Im, H. U.; Lee, H. M.; Yoo, J.-B.; Hong, S.-H.; Kang, T. J.; Kim, Y. H. Flexible Hydrogen Sensors Using Graphene with Palladium Nanoparticle Decoration. *Sens. Actuators, B* **2012**, *169*, 387−392.
(20) Johnson, J. L.; Behnam, A.; Pearton, S. J.; Ural, A. Hydrogen Sensing Using Pd-Functionalized Multi-Layer Graphene Nanoribbon Networks. *Adv. Mater.* **2010**, *22*, 4877−4880.
(21) Mubeen, S.; Zhang, T.; Yoo, B.; Deshusses, M. A.; Myung, N. V. Palladium Nanoparticles Decorated Single-Walled Carbon Nanotube Hydrogen Sensor. *J. Phys. Chem. C* **2007**, *111*, 6321−6327.
(22) Lundstrom, I.; Shivaraman, M. S.; Svensson, C. Chemical Reactions on Palladium Surfaces Studied with Pd-MOS Structures. *Surf. Sci.* **1977**, *64*, 497−519.
(23) Choi, B.-Y.; Pak, Y.; Kim, K. S.; Lee, K.-H.; Jung, G.-Y. Simultaneous Fabrication of Line Defects-Embedded Periodic Lattice by Topographically Assisted Holographic Lithography. *Nanoscale Res. Lett.* **2011**, *6*, 449.
(24) Qi, J. L.; Zheng, W. T.; Zheng, X. H.; Wang, X.; Tian, H. W. Relatively Low Temperature Synthesis of Graphene by Radio Frequency Plasma Enhanced Chemical Vapor Deposition. *Appl. Surf. Sci.* **2011**, *257*, 6531−6534.
(25) Ryu, S.; Liu, L.; Berciaud, S.; Yu, Y.-J.; Liu, H.; Kim, P.; Flynn, G. W.; Brus, L. E. Atmospheric Oxygen Binding and Hole Doping in Deformed Graphene on a $SiO_2$ Substrate. *Nano Lett.* **2010**, *10*, 4944−4951.
(26) Ferrari, A. C.; Meyer, J. C.; Scardaci, V.; Casiraghi, C.; Lazzeri, M.; Mauri, F.; Piscanec, S.; Jiang, D.; Novoselov, K. S.; Roth, S.; Geim, A. K. Raman Spectrum of Graphene and Graphene Layers. *Phys. Rev. Lett.* **2006**, *97*, 187401.
(27) Graf, D.; Molitor, F.; Ensslin, K.; Stampfer, C.; Jungen, A.; Hierold, C.; Wirtz, L. Spatially Resolved Raman Spectroscopy of Single- and Few-Layer Graphene. *Nano Lett.* **2007**, *7*, 238−242.
(28) Wang, Y. Y.; Ni, Z. H.; Yu, T.; Shen, Z. X.; Wang, H. M.; Wu, Y. H.; Chen, W.; Wee, A. T. S. Raman Studies of Monolayer Graphene: The Substrate Effect. *J. Phys. Chem. C* **2008**, *112*, 10637−10640.
(29) Jiao, L.; Zhang, L.; Wang, X.; Diankov, G.; Dai, H. Narrow Graphene Nanoribbons from Carbon Nanotubes. *Nature* **2009**, *458*, 877−880.
(30) Kato, T.; Hatakeyama, R. Site- and Alignment-Controlled Growth of Graphene Nanoribbons from Nickel Nanobars. *Nat. Nanotechnol.* **2012**, *7*, 651−656.
(31) Ghosh, R.; Midya, A.; Santra, S.; Ray, S. K.; Guha, P. K. Chemically Reduced Graphene Oxide for Ammonia Detection at Room Temperature. *ACS Appl. Mater. Interfaces* **2013**, *5*, 7599−7603.
(32) Li, Z.; Wang, Y.; Kozbial, A.; Shenoy, G.; Zhou, F.; McGinley, R.; Ireland, P.; Morganstein, B.; Kunkel, A.; Surwade, S. P.; Li, L.; Liu, H. Effect of Airbone Contaminants on The Wettability of Supported Graphene and Graphite. *Nat. Mater.* **2013**, *12*, 925−931.
(33) Kong, J.; Chapline, M. G.; Dai, H. Functionalized Carbon Nanotubes for Molecular Hydrogen Sensors. *Adv. Mater.* **2001**, *13*, 1384−1386.
(34) Sundaram, R. S.; Gomez-Navarro, C.; Balasubramanian, K.; Burghard, M.; Kern, K. Electrochemical Modification of Graphene. *Adv. Mater.* **2008**, *20*, 3050−3053.
(35) Laider, K. J. *Chemical Kinetics*, 1st ed; McGraw-Hill: New York, 1965.